Diffusion of UV Additives in Ethylene-Vinyl Acetate Copolymer Encapsulants and the Impact on Polymer Reliability

Robert Heidrich, Marius Lüdemann, Anton Mordvinkin, and Ralph Gottschalg

***Abstract*—The reliability of solar modules is largely determined by the encapsulation materials used and their inherent additive composition. Although the use of polymer additives generally leads to better encapsulant characteristics, the diffusion of these species must be considered. While UV additives protect the encapsulant from photo degradation, their interactions with other additives or with formed radicals can lead to undesirable effects such as browning. Within this work, the diffusion of UV additives and their impact on the degradation behavior of encapsulation material based on ethylene-vinyl acetate copolymer (EVA) is investigated. The fabricated test specimens (glass/EVA/PTFE/glass) were prepared with an artificially created UV additive concentration gradient and weathered under IEC 62788-7-2-A3 conditions. Test points with included UV additives showed no degradation effects, while test points without UV additives showed strong degradation. Surprisingly, the UV additives used could diffuse up to 4 cm within 1500 h weathering. They were able to effectively protect an area of 1.3 cm next to the concentration gradient. Therefore, minor inhomogeneities during the manufacturing process can probably be compensated by intrinsic UV additive diffusion. However, this simultaneously represents a high risk of reaction with residual crosslinking peroxides leading to the UV stabilizer depletion and eventually to browning.**

***Index Terms*—Additives, degradation, diffusion, encapsulant, ethylene-vinyl acetate (EVA), spectroscopy.**

I. Introduction

ENCAPSULATION polymer degradation by UV irradiance is known to be one of the key factors determining solar module longevity [1], [2], [3], [4]. Most commonly ethylene-vinyl acetate copolymer (EVA) is used as encapsulant for photovoltaic modules [5]. However, EVA can degrade by various reactions reducing the solar module reliability resulting in browning or the formation of acetic acid, which is corroding contacts and increasing the series resistance and thus seriously influencing the solar module performance [3], [6], [7], [8], [9], [10], [11], [12], [13]. Hence, shielding the encapsulation material by using appropriate additives is a necessary step to enhance the solar module lifetimes [14].

Additives have to fulfill a number of tasks and were used in EVA encapsulants for many decades [15]. While crosslinking additives are important to form a resilient network of polymer chains, unconsumed crosslinking peroxides can cause problems like browning when reacting with other additives [16], [17]. Typically, UV absorbers and UV stabilizers are used to increase the resistance against UV irradiation. Jentsch et al. [14] found that a combination of UV absorbing benzophenone-type molecules and radical trapping hindered amine light stabilizers (HALS) molecules has a synergy effect preventing the encapsulant from photo degradation. On the other hand, correlations between the presence of UV absorbers and browning of the encapsulant have been reported in the literature [6], [16], [18].

Additives can migrate due to diffusion processes [19], [20]. For most cases (e.g., neglecting external forces and convection effects), the description of additive migration by Fick's laws and deriving the general diffusion equation

$$\frac{\partial c}{\partial t} = \vec{\nabla} \cdot \left(D \vec{\nabla} c \right) \tag{1}$$

with c as the molecule concentration, t as the time and D as diffusion constant, is a sufficient approach [19]. In the past, several studies investigated the migration of small molecules in polymer films [21], [22], [23], [24], [25], [26]. Földes et al. [21], [22], [23] determined the diffusion coefficients of different antioxidants in polyolefin polymers. Reynier et al. [25] derived several diffusion coefficients for smaller different molecules and commercial additives in polypropylene. Thus, it is very likely that diffusion effects also occur in EVA layers of commercial solar modules. Furthermore, solar modules are complex physical objects consisting of different materials and various interfaces [3], [9]. Understanding potential interactions between these layers and also the possible migration of smaller species

Manuscript received 31 August 2023; revised 17 October 2023 and 9 November 2023; accepted 10 November 2023. Date of publication 27 November 2023; date of current version 18 December 2023. This work was supported in part by German Research Foundation (Deutsche Forschungsgemeinschaft DFG) under Grant 491460386, in part by the Open Access Publishing Fund of Anhalt University of Applied Sciences, and in part by TotalEnergies. *(Corresponding author: Robert Heidrich.)*

Robert Heidrich is with the Fraunhofer Center for Silicon Photovoltaics CSP, 06120 Halle (Saale), Germany, and also with the Anhalt University of Applied Sciences, 06366 Koethen (Anhalt), Germany (e-mail: robert.heidrich@csp.fraunhofer.de).

Marius Lüdemann and Anton Mordvinkin are with the Fraunhofer Center for Silicon Photovoltaics CSP, 06120 Halle (Saale), Germany (e-mail: marius.luedemann@imws.fraunhofer.de; anton.mordvinkin@csp.fraunhofer.de).

Ralph Gottschalg is with the Fraunhofer Center for Silicon Photovoltaics CSP, 06120 Halle (Saale), Germany, and also with the Anhalt University of Applied Sciences, 06366 Koethen (Anhalt), Germany (e-mail: ralph.gottschalg@csp.fraunhofer.de).

Color versions of one or more figures in this article are available at https://doi.org/10.1109/JPHOTOV.2023.3333198.

Digital Object Identifier 10.1109/JPHOTOV.2023.3333198

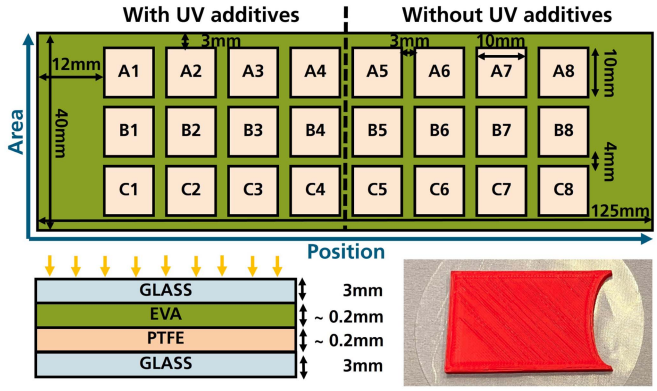

Fig. 1. Top: Sample geometry with all 24 extraction points. Repeatable sample extraction was enabled by using a 3D printed template. Bottom left: Sample cross section showing all used layers with approximate thicknesses and the path of irradiation. Bottom right: Cutting template with an elliptic opening.

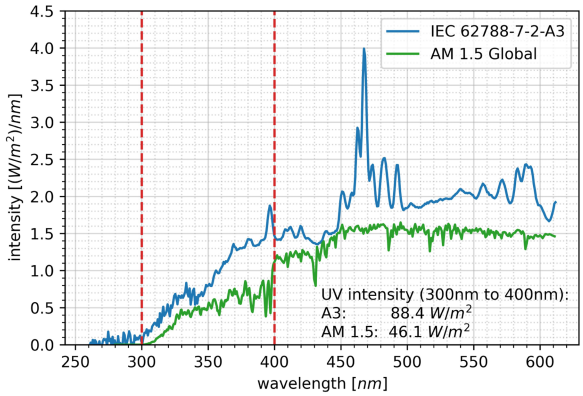

Fig. 2. Spectrum of the used xenon lamps with daylight filters in comparison with the standard spectrum AM 1.5 Global (ASTM G173-03 reference spectra derived from SMARTS v. 2.9.2. provided by NREL).

TABLE I
USED ENCAPSULANT COMPOSITIONS C1 (WITH UV ADDITIVES) AND C2 (WITHOUT UV ADDITIVES)

Name	Function	C1 [phr]	C2 [phr]	CAS
ELVAX 150W	EVA matrix	100	100	
Cyasorb UV 531	UV absorber	0.3	0	1843-05-6
Tinuvin 770	HALS	0.13	0	52829-07-9
Luperox TBEC	crosslinking agent	1.5	1.5	34443-12-4
Perkalink 301	crosslinking accel.	1.5	1.5	1025-15-6
Silane A 174	adhesion promoter	1.2	1.2	2530-85-0

The additive amounts are presented in grams per hundred gram EVA.

between different films is crucial for determining the longevity of the materials. On the one hand, this means that diffusion of additives from the initial site reduces the protection of the encapsulation material against environmental influences. On the other hand, initial inhomogeneities in the additive density could be compensated by diffusion effects.

This work aims to investigate the influence of UV additives on the degradation behavior of EVA films and to analyze potential diffusion effects. For this purpose, diffusion specimens, with 24 measurement points each, were manufactured. The weathering took place in rondel weatherometers under IEC 62788-7-2-A3 conditions. The newly developed quantification method for UV additives in EVA by pyrolysis-gas chromatography-mass spectrometry (PY-GCMS) will enable a time and spatially resolved determination of the corresponding UV additive concentration [27].

II. MATERIALS AND METHODS

A. Used Materials and Sample Manufacturing

Fig. 1 visualizes the sample design. *Position* represents the sites 1 to 8 along the sample length. *Area* represents the sites A to C along the sample width. The EVA films have been manufactured in accordance with our previous work using a kneader and a hydraulic press [27]. Two different EVA types were prepared with a common additive structure while the presence of UV additives was varied [15], [18], [27], [28]. The formulations are displayed in Table I. After the pressing process, the samples were equally cut with the help of a template (see Fig. 1). Preliminary lamination experiments have shown that an elliptic form of the interface, where the different polymer films are laminated together, is beneficial as the EVA is flowing faster in the middle of the glass substrate.

Subsequently, two EVA films (one with, one without UV additives) were positioned on low iron, thermally hardened float glass and covered with a PTFE layer to enable the separation after weathering. After placing a second glass layer on top, the samples were laminated. An Meier ICOLAM 10/08 was used for lamination. The laminator was pre heated to 55 °C. Afterward, all samples were placed inside the laminator. The laminator was evacuated for 6.5 min and heated to 80 °C. Afterward, the coupons were pressed with 600 mbar and heated to 155 °C within 3 min. The temperature and pressure were hold for additional 15 min. In the last step the laminator was cooled to 55 °C within 30 min still applying the 600 mbar pressure.

After the lamination process aluminum tape was used to seal the edges of all glass laminates to exclude the influence of humidity and oxygen. Additionally, a template containing the openings as shown in Fig. 1 was 3D printed, allowing a reproducible sample extraction from the same points.

B. Weathering

The weathering was carried out in accordance with IEC 62788-7-2-A3 using an Atlas Xenotest 440 with Atlas B04 daylight filters. The chamber temperature was fixed at 65 °C (90 °C black standard temperature) with 20 % relative humidity. The Intensity at 340 nm was set to 0.8 $\mathrm{W/m^2/nm}$. The measured spectrum is displayed in Fig. 2. Especially the UV interval of the xenon lamp with daylight filters behaves similar to the AM 1.5 Global, but the integrated intensity is increased by approximately the doubled amount. However, the spectrometer was not calibrated to the chamber geometry. Therefore, the measured (and integrated) intensities are slightly higher than displayed in the chamber parameters and should be understood qualitatively. All samples were irradiated with EVA as top layer in accordance with Fig. 1.

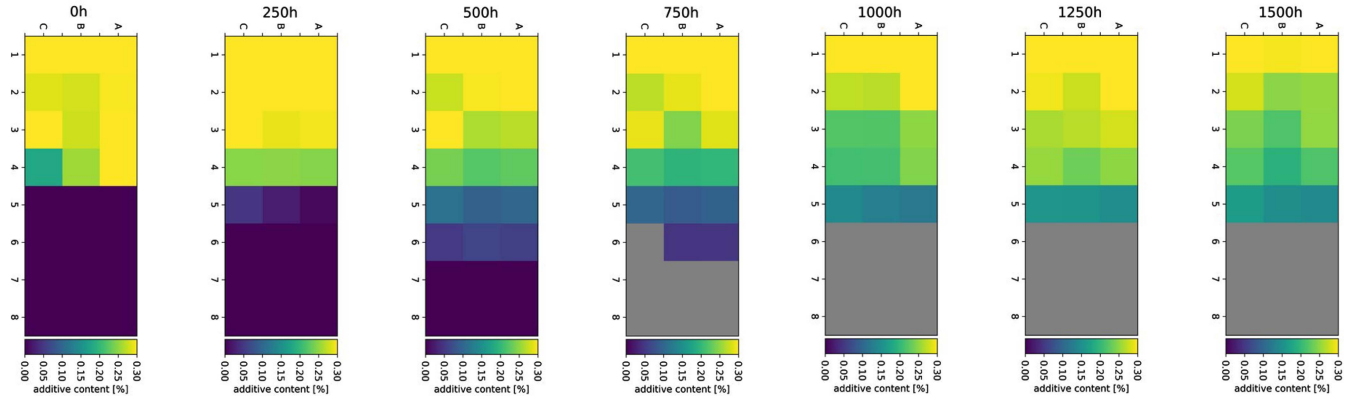

Fig. 3. Quantification of the UV absorber Cyasorb UV 531. The map positioning is in accordance with Fig. 1. Evaluation of the gray area and position combinations were not possible due to serious degradation.

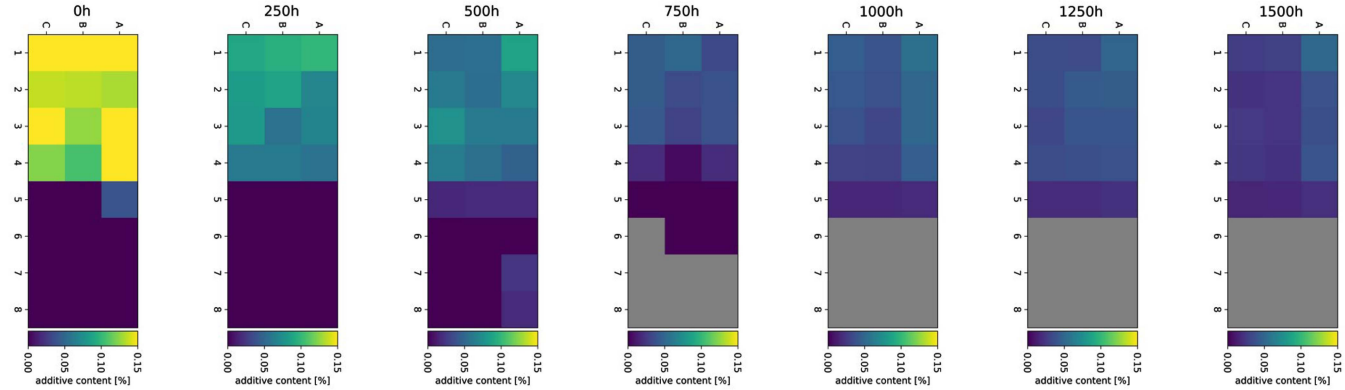

Fig. 4. Quantification of the UV stabilizer Tinuvin 770. The map positioning is in accordance with Fig. 1. Evaluation of the gray area and position combinations were not possible due to serious degradation.

C. Characterization Methods

1) Pyrolysis-Gas Chromatography-Mass Spectrometry (PY-GCMS): For qualitative and quantitative analysis of the polymer and the additive composition a combination of pyrolysis, gas chromatography and mass spectrometry (PY-GCMS) was used. The PY-GCMS setup and quantification procedure are explained in detail in our previous work focusing on additive quantification [27]. An EGA/Py-3030D from Frontier Laboratories Ltd. pyrolysis oven with attached autosampler AS-1020E was used for a two step thermo desorption. All desorption steps were carried out with the help of a selective sampler SS-1010E from Frontier Laboratories Ltd., which prevents column contamination by undesirable fragmented components. As gas chromatograph a Trace 1300 from Thermo Scientific with He carrier gas was used. The implemented column was an Ultra ALLOY Capillary Column (length $30\,\mathrm{m}$, internal diameter $0.25\,\mathrm{mm}$, film thickness $0.25\,\mu\mathrm{m}$) from Frontier Laboratories Ltd. An ISQ 7000 mass spectrometer from Thermo Scientific was coupled to the gas chromatograph. The m/z range was set from 29 to 800.

2) Fourier-Transform Infrared Spectroscopy (FTIR): An Inventio spectrometer from Bruker was used for the FTIR analysis. The measurements were carried out in ATR mode using a transit platinum unit with diamond tip. The wavelength interval was set from $4000\,\mathrm{cm}^{-1}$ to $650\,\mathrm{cm}^{-1}$ with a resolution of $4\,\mathrm{cm}^{-1}$.

III. Results and Discussion

A. Additive Diffusion

Figs. 3 and 4 are visualizing the quantitative PY-GCMS analysis of the UV absorber Cyasorb UV 531 and the UV stabilizer Tinuvin 770. Comparing the initial values with Table I, the UV stabilizer exaggerated in the samples during the initial state. This could either be caused by local inhomogeneities as a result of the kneader fabrication or by a general offset due to the calibration samples for PY-GCMS quantification [27]. However, comparing relative mass changes is possible with sufficient accuracy. Not all defined samples positions were analyzed until the end of the weathering time. The gray color in Figs. 3 and 4 symbolizes encapsulant position and area combinations, which were subject to severe degradation which impeded PY-GCMS measurements (see Fig. 9) and will be discussed in Section III-B. Due the diverging modes of operation of the UV absorber and the UV stabilizer, the mean content of both molecules relative to the total sample surface behaves differently and is shown for position 1 to 5 in Fig. 5.

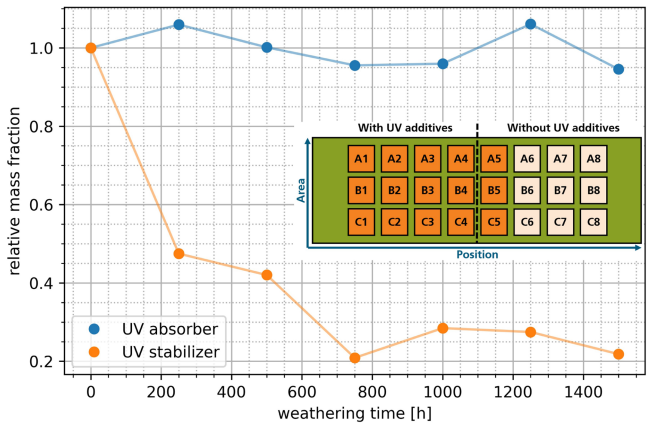

Fig. 5. Mean relative additive content of the UV absorber Cyasorb UV 531 and the UV stabilizer Tinuvin 770 for positions 1 to 5 (mean of all orange extraction points in the scheme). Considering Figs. 3 and 4, the total amount of the UV absorber in position 1 to 5 is preserved but redistributed. The total amount of the UV stabilizer is drastically decreasing within the first 250 h of weathering.

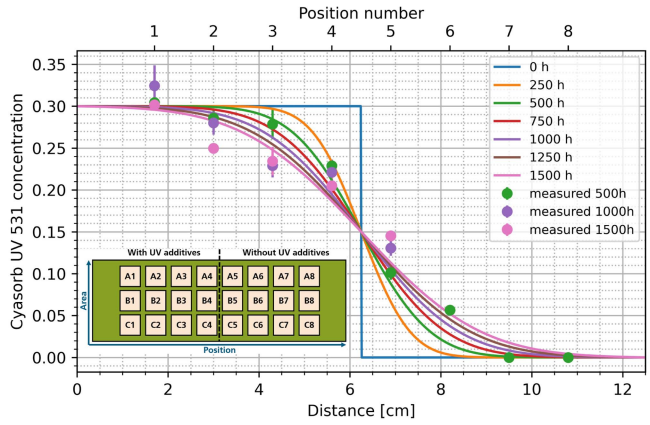

Fig. 6. Numerical solution of the diffusion equation for the UV absorber Cyasorb UV 531. The problem was simplified to a 1D simulation, and the measurement points are mean values of area A to C at the corresponding position. The error bars represent the standard deviation of the mean values.

Fig. 3 shows that UV absorber molecules start to diffuse significantly from position 4 as the concentration gradient is the highest, which is in accordance with general macroscopic Fickian diffusion [19]. After 250 h of weathering the UV absorber already diffused into position 6 and and is expected to diffuse further. However, further positions could not be analyzed due to the aforementioned polymer degradation. Due to the changing concentration gradient molecules from the positions 2 and 3 are predominantly compensating the concentration mismatch and after 1500 h only position 1 remained with approximately the initial concentration. Considering the mean relative additive content of position 1 to 5, which is displayed in Fig. 5, the total UV absorber content remains approximately constant. Therefore, the underlying keto-enol tautomerism works reversible for the applied weathering parameters and the total amount of the UV absorber is preserved but redistributed [7], [29], [30].

Thus, the general diffusion equation approach

$$\frac{\partial u(x,t)}{\partial t} = D\frac{\partial^2 u(x,t)}{\partial x^2} \tag{2}$$

was assumed for the UV absorber as displayed in (2) with $u(x,t)$ as UV absorber concentration and D as diffusion constant. The partial differential equation was solved numerically using an explicit forward in time and central in space (FTCS) approach with Dirichlet conditions for the boundary with UV additives and Neumann conditions for the boundary without UV additives. Both conditions have been chosen to match the observations as the initial concentration in position 1 remained constant while the additives cannot diffuse out of the sample on the other side. The effect of encapsulant thickness was not examined in this study as the numerical diffusion simulation was simplified to 1D for symmetry reasons, because no additional information could be gained in the case of a 2D observation. In the course of simplification to a 1D problem, the mean value of the areas A, B, and C for every position 1 to 8 was used. Fig. 6 shows the results of the numerical simulation and the real measured data points of the 500 h sample, the 1000 h sample and the 1500 h sample. When using a diffusion constant of $D = 5.5 \times 10^{-8}\,\mathrm{cm^2/s}$, the measured data points show a good agreement with the simulation. This value is in accordance with the work of Reynier et al. who determined the diffusion constant of Cyasorb UV 531 (Chimassorb 81) in polypropylene between $1.5 \times 10^{-10}\,\mathrm{cm^2/s}$ (40 °C) and $1.4 \times 10^{-8}\,\mathrm{cm^2/s}$ (70 °C) [25]. As the chamber and sample temperature (both temperatures should be approximately equal due to the transparent sample laminates [31], [32]) are approximately 65 °C during weathering, the used diffusion constant is in the correct order of magnitude. In addition, Földes et al. [21], [22], [23] determined similar diffusion coefficients for different antioxidants migrating in EVA. In accordance with the measured values, the graph shows that after 500 h the concentration in position 5 is increased to 1/3 of the initial concentration. After 1500 h of weathering, position 5 reached approximately half of the base concentration. Thus, under the used weathering parameters, the UV absorber is could be able to migrate approximately 4 cm within 1500 h of weathering.

However, the deviations of the measurements from the simulation could also be a result of an anomalous diffusion of the UV absorber. The normal diffusion and anomalous diffusion for the 1D case are displayed in (3) and (4). Assuming Fickian (normal) diffusion, the mean squared displacement

$$\langle r^2(t)\rangle = 2Dt \tag{3}$$

should allow particle movements of approximately 0.77 cm within 1500 h of weathering, which is significantly smaller than the measured data points and the simulation [33], [34]. Thus, D could be concentration dependent indicating a super diffusive behavior of the UV absorber [35], [36], [37], [38]. Following the anomalous diffusion approach

$$\langle r^2(t)\rangle = 2D_\alpha t^\alpha \tag{4}$$

with the anomaly parameter α for the measured data of the 500 h time step (and a mean square displacement of 2^2 cm^2—see Fig. 6), the given diffusion constant of $5.5 \times 10^{-8}\,\mathrm{cm^2/s}$ would result in $\alpha = 1.21$ [38].

In order to exclude the influence of the PTFE layer on the diffusion behavior of the additives, samples from the same series were further weathered up to 2000 h. No additives were detected in the bulk measurements of the PFTE layers, but significant amounts were still found in the EVA. Consequently, the PTFE layer does not contribute to the transport of additives, neither on its surface nor within its volume. As an explanation for the anomalous diffusion, the incomplete EVA crosslinking can be responsible. Typically, EVA features a maximum gel content of 90 %, meaning that 10 % of the material can flow, which can accelerate the additive diffusion leading to the superdiffusion regime [39]. The vinyl acetate (VA) content can also play a role in this assumption. A lower VA content leads to higher crystallinity and lower glass transition temperature. Thus, the former would slow down, whereas the latter would boost the diffusion of additives in the polymer matrix [40], [41].

The migration of UV stabilizer molecules displayed in Fig. 4 behaves differently. While the migration due to the convectional transport associated with the material flow was already detected directly after the lamination (0 h sample), the diffusion effects are in general much less pronounced. In addition, after 250 h the initial concentration is approximately halved for all points, with position 4 showing the highest decrease. This could be explained by the reaction of the UV stabilizer with residual crosslinking peroxides which were not consumed during lamination and will be discussed in more detail in Section III-B. While the 500 h sample shows migration into position 5, this molecule diffusion is not detected for the 750 h sample. The observed behavior can be explained by a superposition of two effects. While the general concept of additive diffusion should also be applicable for Tinuvin 770, the migration of additives into new positions is probably counterbalanced by their reaction with radicals as their mode of action is not reversible [42], [43], [44], [45].

The molecular weight of the UV stabilizer Tinuvin 770 is 481 g/mol [46]. Földes et al. [22] found the diffusion coefficient of the antioxidant Irganox 1076 with a molecular weight of 531 g/mol to be $2.7 \times 10^{-8}\,\mathrm{cm^2/s}$ in EVA at 80 °C. As the molecular weight of the UV absorber Cyasorb UV 531 is 326 g/mol ($D = 5.5 \times 10^{-8}\,\mathrm{cm^2/s}$), it is conceivable that the diffusion coefficient of Tinuvin 770 is in the same order of magnitude as the previous mentioned additives [46]. As displayed in Fig. 5, the total UV stabilizer content is decreasing rapidly. Assuming a reservoir of formed radicals by UV irradiation (or nonconsumed crosslinking peroxide radicals), the degradation kinetics of the HALS should be dependent on their total amount as they need a reaction partner. Thus, the quantified HALS base form degrades with first order kinetics leading to an exponential decay of the total UV stabilizer concentration, which is observable in Fig. 5. As a result, the total Tinuvin 770 base form concentration decreased to approximately 20 % of the initial concentration after 1500 h of weathering. However, the decrease of molecular concentration (especially in position 1 to 4) does not necessarily mean the stabilizer is not functional anymore. As stated by Hodgeson et al. [44] the Denisov cycle is complex and even HALS fragments are able to bind radicals as long as the functional amine group is present.

TABLE II
FTIR ABSORPTION PEAK ASSIGNMENT

waven. [$\mathrm{cm^{-1}}$]	group	excitation
3700-3100	OH	stretching vibration of hydroxyl groups
2920	CH_2	stretching vibration (PE)
2850	CH_2	deformation vibration (PE)
1900-1780	C=O	stretching vibration of γ-lactones
1736	C=O	stretching vibration (VA)
1715-1600	C=O	stretching vibration of ketones
1465	CH_2	stretching vibration (PE)
1370	CH_3	deformation vibration (VA)
1238	C-O-C	stretching vibration (VA)
1170	C-O-C	stretching vibration of aliphatic esters
1020	C-O-C	stretching vibration (VA)
960	CH	deformation vibration
720	CH_2	skeleton rocking vibration (PE)

Intensities belong to the polyethylene (PE) units, the vinyl acetate (VA) units or degradation products of the base polymer. The assignment is in accordance with [48], [49], [50], [8], [51], [52].

B. EVA Degradation in Dependence of UV Additive Presence

The EVA degradation was analyzed with ATR-FTIR measurements. All presented spectra are mean values of one position (e.g., the mean value of A1, B1, C1, etc.). Table II lists all assigned peaks with the corresponding functional group. Here, the peaks at 2920 $\mathrm{cm^{-1}}$, 2850 $\mathrm{cm^{-1}}$, 1465 $\mathrm{cm^{-1}}$, and 720 $\mathrm{cm^{-1}}$ belong to the polyethylene (PE) units. The peaks at 1736 $\mathrm{cm^{-1}}$, 1370 $\mathrm{cm^{-1}}$, 1238 $\mathrm{cm^{-1}}$, and 1020 $\mathrm{cm^{-1}}$ are assigned to the vinyl acetate (VA) units. The changes of the absorption bands in dependence of weathering time for the positions 3, 5, and 6 are displayed in Figs. 7 and 8. In addition, the oxidation index (OI) was calculated using the ratio of the wavenumber dependent absorption $A(k)$ of the 1736 $\mathrm{cm^{-1}}$ C=O peak and the 1465 $\mathrm{cm^{-1}}$ CH_2 peak [47]

$$OI = \frac{\int_{1600}^{1900} A(k)\mathrm{d}k}{\int_{1400}^{1500} A(k)\mathrm{d}k} \tag{5}$$

and displayed in the right image of Fig. 8.

Within 1500 h of weathering, position 3 did not show changes of the chemical structure. The OI remained approximately constant while small changes are probably rather a result of inhomegneities between the different samples than an aging effect. Considering the quantification of the UV additives in position 3, the UV absorber amount is still approximately 83 % of the initial concentration. Also, the UV stabilizer should be still functional, which has probably led to a suppression of degradation effects.

A similar result can be reported for position 5. The OI is slightly increased by approximately 20 % in comparison with the initial value after 1500 h of weathering. In addition, the broadening of the peak shoulder at 1715 $\mathrm{cm^{-1}}$ suggests the formation of ketones as a result of the degradation of the vinyl acetate entity [8], [49], [50], [51], [52]. However, considering the previously carried out quantification, the migration of UV additives was significantly damping the effects of photo degradation. Taking Fig. 6 into account, the UV absorber content in position 5 reached approximately 23 % of the initial concentration within 250 h. Based on the previous argumentation, it is conceivable that a similar amount of HALS additives also migrated to position 3, but was directly consumed by the formed

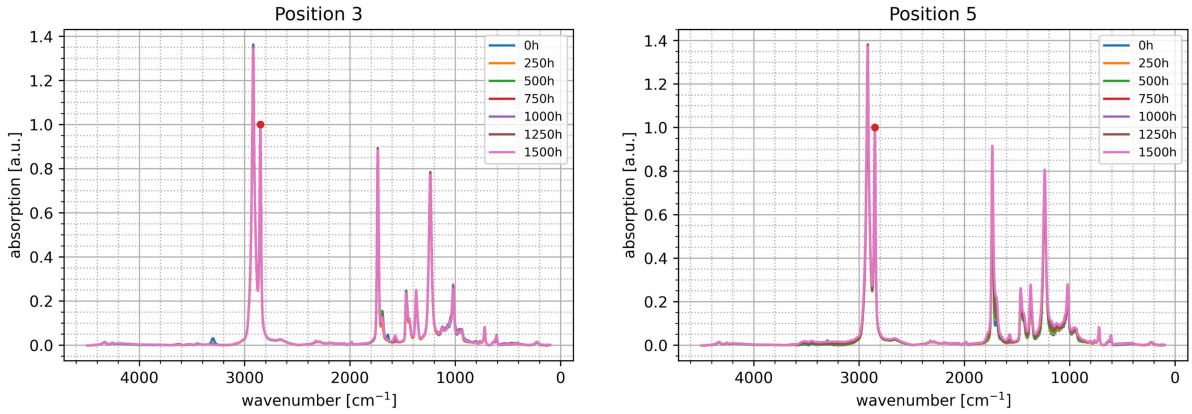

Fig. 7. FTIR measurements of the position 3 (left–with UV additives) and the position 5 (right – initially without UV additives) in dependence of weathering time. All spectra are mean values of the areas A, B, and C. The data was normalized to the 2850 cm^{-1} CH_2 peak (marked with the red dot).

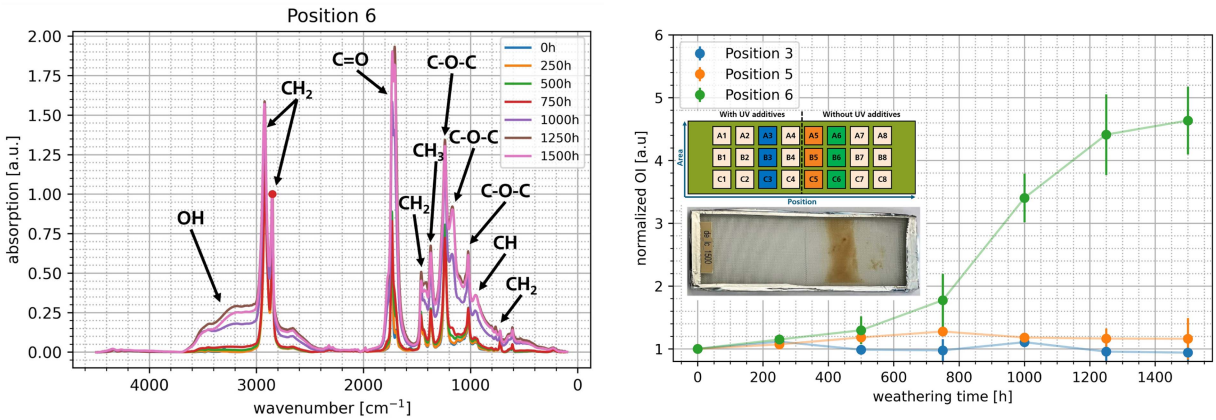

Fig. 8. FTIR measurements of the position 6 (left–without UV additives) and the development of the oxidation index (right) in dependence of weathering time. All data are mean values of the areas A, B, and C. The data was normalized to the 2850 cm^{-1} CH_2 peak (marked with the red dot) for the FTIR spectrum and to the initial oxidation index for the OI development.

radicals. Nevertheless, the migration UV additives forced by a concentration gradient was able to effectively prohibit photo degradation within 1.3 cm of lateral space.

Comparing these results with the spectrum of Position 6 in Fig. 8, the importance of UV additives becomes obvious. After 750 h of aging, the formation of several groups occurred. The formation of OH bonds can be found from 3700 cm^{-1} to 3100 cm^{-1}. These interactions are created by hydroperoxides or by hydroxyl groups as a result of hydroperoxide breakdown and are discussed in [49] and [50]. The peak shoulder from 1900 cm^{-1} to 1780 cm^{-1} is significantly broadened which is caused by γ-lactones [8], [49], [51]. These species are formed by the degradation of the VA units through the back-biting process [8], [49]. The other peak shoulder of the C=O peak from 1715 cm^{-1} to 1600 cm^{-1} is also broadened, which is caused by the generation of ketones [8], [49], [50], [51], [52]. They are either formed by Norrish type III reactions or due to the breakdown of hydroperoxides [8]. At 1170 cm^{-1}, a new peak was formed after 750 h of weathering. The C-O-C interaction is probably a result of the formation of aliphatic esters or as a result of the chain scission [8], [49], [51]. In addition, the absorption at 960 cm^{-1} intensified. These intensities are cause by CH out of plane bending. They occur in species like R-CH=CH-R which form during deacetylation [49]. In accordance with the changes in the spectra after 750 h of weathering, the OI started to increase significantly. After 1250 h of weathering the EVA was nearly totally degraded and a saturation of the OI increase occurred. The OI finally increased to approximately 4.6 times of the initial value after 1500 h due to ketone and lactone formation.

Fig. 9 visualizes the diffusion sample after 1500 h of weathering. Positions 1 to 5 do not show visual photo degradation. In position 6, severe browning occurred. However, these browning effects are not visible from position 7 to the end of the sample side without UV additives. Nevertheless, the removed samples from positions 6 to 8 were in a jellylike condition suggesting the destruction of the polymer network. In the literature, the presence of chromophores is correlated with the formation of

Fig. 9. Sample extracted after 1500 h of weathering. The sample extraction points with UV additives and without UV additives are in accordance with Fig. 1. Especially position 6 shows severe browning.

C=C and C=O bonds [1], [6], [7], [49], [53], [54]. While C=C bonds are also presented within the moieties generating the absorption intensities at 960 cm^{-1}, they should equally form in all positions without UV additives. Thus, the formed C=C bonds are probably no indication for the formation of chromophores, which are causing the browning effect.

On the other hand, several groups found correlations of additive presence and chromophore formation [6], [16], [18], [55], [56], [57], [58]. Considering the diffusion samples as displayed in Fig. 9, only the UV additives have been varied between both sides. Klemchuk et al. [16] proposed the formation of chromophore precursors if crosslinking peroxides are not fully consumed during lamination. The crosslinking peroxide reacts with the OH group of the benzophenone UV absorber creating a radical. In the next step, the created radical is interacting with another UV absorber radical to form a larger molecule, which can act as a chromophore [16]. Additionally, Oreski et al. [17] found that nonreacted crosslinking peroxides after lamination can cause browning effects during accelerated aging. Thus, the browning effect is most likely a result of the interactions with the UV absorber Cyasorb UV 531 [6], [16], [18], [58]. For the displayed diffusion samples two scenarios are conceivable while scenario 2) is considered more likely for the presented experiments.

1) The chromophores are formed by the reaction of the UV absorber Cyasorb UV 531 and radicals of the base polymer which are created by UV irradiance in the positions 5 to 8. In position 5, these radicals were neutralized by the UV stabilizer Tinuvin 770. However, the effective range of the UV stabilizer was limited to that position as it was discussed in Section III-A.
2) The chromophores are formed by the reaction of the UV absorber Cyasorb UV 531 with crosslinking peroxides, which were not consumed during the lamination process. During the weathering, the peroxides are radicalized by UV irradiation and react with the migrated UV absorber. This consideration could also explain why the UV stabilizer content was drastically reduced within the first 250 h of weathering (see Fig. 4) as it was consumed by the reaction with peroxide radicals. As in case 1), the effective range of the UV stabilizer was limited to the positions 1 to 5. Thus, the generation of browning effects is dependent on the migration behavior of the UV stabilizer which is in accordance with Fig. 6.

IV. Conclusion

The conducted experiments show the important role of UV additives within EVA encapsulants to prevent UV induced polymer degradation. Positions which have been stabilized by UV additives did not show degradation within 1500 h of weathering under IEC 62788-7-2-A3 conditions. Furthermore, inhomogeneities of the additive density can be balanced effectively by diffusion for distances of approximately 1.3 cm. Thus, positions which did not contain UV additives at the beginning were shielded for the full weathering duration when laying inside the effective distance. A synergy effect of the UV absorber and the UV stabilizer is likely to occur. Positions which have not been stabilized by the UV additives degrade significantly within 750 h of weathering. The formation of hydroxyl groups, ketones, lactones, and aliphatic esters was detected, and the oxidation index was strongly increased.

In total, the UV absorber is probably able to migrate approximately 4 cm within 1500 h of weathering. Considering the previous work by Reynier et al. and Földes et al., it is conceivable that molecules with comparable molecular weights can migrate similar distances when no other interaction occurs. Furthermore, the total UV absorber amount was conserved suggesting reversible keto-enol tautomerism. However, with the used weathering time of 1500 h within the conducted study, it is not possible to conclude whether the number or concentration of used UV-related additives is sufficient. Further experiments with longer weathering times and other combinations of stressors should be carried out to investigate the degradation behavior of the additives and polymers. In addition, the influence of the vinyl acetate content and the diffusion behavior of additives in POE and TPO encapsulants should be investigated at different temperatures and irradiation conditions. As discussed for anomalous diffusion, the microscopic structure of the respective material can have an influence on the migration behavior of different species.

The use of additives is a double edged sword. While the addition of additives is in general necessary for crosslinking reactions and to achieve a reasonable protection from UV irridiance, several interactions must be considered. On the one hand, the diffusion of additives can seemingly have a positive effect of leveling out the additive concentration screening with time the areas initially unprotected. On the other hand, if the crosslinking peroxide is not fully consumed during the lamination process, remnant molecules could decompose by UV irradiance forming radicals. These radicals probably significantly consume the UV stabilizer content. Moreover, they react with the UV absorber forming chromophores and therefore lead to severe browning effects. Thus, the lamination process or rather the crosslinking peroxide content has to be optimized when benzophenone UV absorbers are used. Either one needs to ideally consume all the peroxides during lamination or a sufficient amount of UV stabilizer needs to be added to trap remaining peroxide radicals.

The experiments within this work discussed effects within one EVA layer and while excluding humidity influences. A real solar module is much more complex as it contains several layers and interfaces with interaction potential. Furthermore, a combination of different stress factors like thermo-mechanical stresses, humidity, and UV irradiance can occur. Within a solar module lifetime, it is very likely that additives from different layers can migrate in the scale of several centimeters. This is especially problematic, when additives interact with each other or with radicals and should also be considered for the emerging EVA/polyolefin/EVA encapsulants. In the case of the UV absorber, the molecules could diffuse from the back side EVA into the front side EVA in solar modules. First, this could lead to a performance decrease because absorbed photons cannot reach the solar cell. Second, the migrated UV absorber molecules could react with radicals forming chromophores and reducing the solar module efficiency even more. Consequently, further studies should address the diffusion behavior of the additives at a coupon level and in solar modules as well as consider different film thicknesses.

REFERENCES

[1] H. Han et al., "Analysis of the degradation of encapsulant materials used in photovoltaic modules exposed to different climates in China," *Sol. Energy*, vol. 194, pp. 177–188, 2019.

[2] A. Czanderna and F. Pern, "Encapsulation of PV modules using ethylene vinyl acetate copolymer as a pottant: A critical review," *Sol. energy Mater. Sol. cells*, vol. 43, no. 2, pp. 101–181, 1996.

[3] M. C. C. de Oliveira, A. S. A. D. Cardoso, M. M. Viana, and V. d. F. C. Lins, "The causes and effects of degradation of encapsulant ethylene vinyl acetate copolymer (EVA) in crystalline silicon photovoltaic modules: A review," *Renewable Sustain. Energy Rev.*, vol. 81, pp. 2299–2317, 2018.

[4] M. Halwachs et al., "Statistical evaluation of pv system performance and failure data among different climate zones," *Renewable Energy*, vol. 139, pp. 1040–1060, 2019.

[5] G. Oreski et al., "Properties and degradation behaviour of polyolefin encapsulants for photovoltaic modules," *Prog. Photovolt., Res. Appl.*, vol. 28, no. 12, pp. 1277–1288, 2020.

[6] F. Pern, "Factors that affect the EVA encapsulant discoloration rate upon accelerated exposure," *Sol. Energy Mater. Sol. Cells*, vol. 41, pp. 587–615, 1996.

[7] F. Pern, "Ethylene-vinyl acetate (EVA) encapsulants for photovoltaic modules: Degradation and discoloration mechanisms and formulation modifications for improved photostability," *Die Angewandte Makromolekulare Chemie: Appl. Macromol. Chem. Phys.*, vol. 252, no. 1, pp. 195–216, 1997.

[8] J. Jin, S. Chen, and J. Zhang, "UV aging behaviour of ethylene-vinyl acetate copolymers (EVA) with different vinyl acetate contents," *Polym. Degradation Stability*, vol. 95, no. 5, pp. 725–732, 2010.

[9] A. Omazic et al., "Relation between degradation of polymeric components in crystalline silicon PV module and climatic conditions: A literature review," *Sol. Energy Mater. Sol. Cells*, vol. 192, pp. 123–133, 2019.

[10] S. Chattopadhyay et al., "Visual degradation in field-aged crystalline silicon PV modules in India and correlation with electrical degradation," *IEEE J. Photovolt.*, vol. 4, no. 6, pp. 1470–1476, Nov. 2014.

[11] A. Sinha, O. Sastry, and R. Gupta, "Nondestructive characterization of encapsulant discoloration effects in crystalline-silicon pv modules," *Sol. Energy Mater. Sol. Cells*, vol. 155, pp. 234–242, 2016.

[12] C. Peike et al., "Origin of damp-heat induced cell degradation," *Sol. Energy Mater. Sol. Cells*, vol. 116, pp. 49–54, 2013.

[13] A. Kraft et al., "Investigation of acetic acid corrosion impact on printed solar cell contacts," *IEEE J. Photovolt.*, vol. 5, no. 3, pp. 736–743, May 2015.

[14] A. Jentsch, K.-J. Eichhorn, and B. Voit, "Influence of typical stabilizers on the aging behavior of EVA foils for photovoltaic applications during artificial UV-weathering," *Polym. Testing*, vol. 44, pp. 242–247, 2015.

[15] E. Cuddihy, C. Coulbert, A. Gupta, and R. Liang, "Flat-plate solar array project. Volume 7: Module encapsulation," 1986.

[16] P. Klemchuk et al., "Investigation of the degradation and stabilization of eva-based encapsulant in field-aged solar energy modules," *Polym. Degradation Stability*, vol. 55, no. 3, pp. 347–365, 1997.

[17] G. Oreski et al., "Crosslinking and post-crosslinking of ethylene vinyl acetate in photovoltaic modules," *J. Appl. Polym. Sci.*, vol. 134, no. 23, 2017.

[18] C. Peike, L. Purschke, K.-A. Weiss, M. Köhl, and M. Kempe, "Towards the origin of photochemical EVA discoloration," in *Proc. IEEE 39th Photovoltaic Specialists Conf.*, 2013, pp. 1579–1584.

[19] H. Frisch and S. A. Stern, "Diffusion of small molecules in polymers," *Crit. Rev. Solid State Mater. Sci.*, vol. 11, no. 2, pp. 123–187, 1983.

[20] J. Sax and J. Ottino, "Modeling of transport of small molecules in polymer blends: Application of effective medium theory," *Polym. Eng. Sci.*, vol. 23, no. 3, pp. 165–176, 1983.

[21] E. Földes and B. Turcsányi, "Transport of small molecules in polyolefins. I. diffusion of irganox 1010 in polyethylene," *J. Appl. Polym. Sci.*, vol. 46, no. 3, pp. 507–515, 1992.

[22] E. Földes, "Transport of small molecules in polyolefins. II. diffusion and solubility of irganox 1076 in ethylene polymers," *J. Appl. Polym. Sci.*, vol. 48, no. 11, pp. 1905–1913, 1993.

[23] E. Földes, "Transport of small molecules in polyolefins. iii. diffusion of topanol ca in ethylene polymers," *J. Appl. Polym. Sci.*, vol. 51, no. 9, pp. 1581–1589, 1994.

[24] S. X. Chen and R. T. Lostritto, "Diffusion of benzocaine in poly (ethylene-vinyl acetate) membranes: Effects of vehicle ethanol concentration and membrane vinyl acetate content," *J. Controlled Release*, vol. 38, no. 2–3, pp. 185–191, 1996.

[25] A. Reynier, P. Dole, and A. Feigenbaum, "Additive diffusion coefficients in polyolefins. ii. effect of swelling and temperature on the d= f (m) correlation," *J. Appl. Polym. Sci.*, vol. 82, no. 10, pp. 2434–2443, 2001.

[26] P. V. Yaneff, K. Adamsons, N. Cliff, and M. Kanouni, "Migration of reactable UVAS and HALS in automotive plastic coatings," *JCT Res.*, vol. 1, pp. 201–212, 2004.

[27] R. Heidrich, A. Mordvinkin, and R. Gottschalg, "Quantification of UV protecting additives in ethylene-vinyl acetate copolymer encapsulants for photovoltaic modules with pyrolysis-gas chromatography-mass spectrometry," *Polym. Testing*, vol. 118, 2023, Art. no. 107913.

[28] A. Beinert et al., "The influence of the additive composition on degradation induced changes in poly (ethylene-co-vinyl acetate) during photochemical aging," in *Proc. 29th Eur. PV Sol. Energy Conf. Exhib.*, Amsterdam, 2014.

[29] N. A. Shaath, "Ultraviolet filters," *Photochemical Photobiological Sci.*, vol. 9, pp. 464–469, 2010.

[30] J. Zawadiak and M. Mrzyczek, "Influence of substituent on uv absorption and keto–enol tautomerism equilibrium of dibenzoylmethane derivatives," *Spectrochimica Acta Part A: Mol. Biomol. Spectrosc.*, vol. 96, pp. 815–819, 2012.

[31] J. Pickett, D. Gibson, S. Rice, and M. Gardner, "Effects of temperature on the weathering of engineering thermoplastics," *Polym. Degradation Stability*, vol. 93, no. 3, pp. 684–691, 2008.

[32] J. E. Pickett and J. R. Sargent, "Sample temperatures during outdoor and laboratory weathering exposures," *Polym. Degradation Stability*, vol. 94, no. 2, pp. 189–195, 2009.

[33] A. Einstein, "Über die von der molekularkinetischen theorie der wärme geforderte bewegung von in ruhenden flüssigkeiten suspendierten teilchen," *Annalen der physik*, vol. 4, pp. 549–560, 1905.

[34] M. V. Smoluchowski, "Zur kinetischen theorie der brownschen molekularbewegung und der suspensionen," *Annalen der physik*, vol. 326, no. 14, pp. 756–780, 1906.

[35] C. M. Hansen, "Diffusion in polymers," *Polym. Eng. Sci.*, vol. 20, no. 4, pp. 252–258, 1980.

[36] S. Havlin and D. Ben-Avraham, "Diffusion in disordered media," *Adv. Phys.*, vol. 36, no. 6, pp. 695–798, 1987.

[37] F. Müller-Plathe, S. C. Rogers, and W. F. van Gunsteren, "Computational evidence for anomalous diffusion of small molecules in amorphous polymers," *Chem. Phys. Lett.*, vol. 199, no. 3–4, pp. 237–243, 1992.

[38] R. Metzler and J. Klafter, "The random walk's guide to anomalous diffusion: A fractional dynamics approach," *Phys. Rep.*, vol. 339, no. 1, pp. 1–77, 2000.

[39] M. Jaunich, M. Böhning, U. Braun, G. Teteris, and W. Stark, "Investigation of the curing state of ethylene/vinyl acetate copolymer (EVA) for photovoltaic applications by gel content determination, rheology, DSC and FTIR," *Polym. Testing*, vol. 52, pp. 133–140, 2016.

[40] M. Brogly, M. Nardin, and J. Schultz, "Effect of vinylacetate content on crystallinity and second-order transitions in ethylene—vinylacetate copolymers," *J. Appl. Polym. Sci.*, vol. 64, no. 10, pp. 1903–1912, 1997.

[41] J. S. Puente et al., "Segmental mobility and glass transition of poly (ethylene-vinyl acetate) copolymers: Is there a continuum in the dynamic glass transitions from PVAC to pe ?," *Polymer*, vol. 76, pp. 213–219, 2015.
[42] E. Denisov, "The role and reactions of nitroxyl radicals in hindered piperidine light stabilisation," *Polym. Degradation Stability*, vol. 34, no. 1–3, pp. 325–332, 1991.
[43] E. N. Step, N. J. Turro, P. P. Klemchuk, and M. E. Gande, "Model studies on the mechanism of hals stabilization," *Die Angewandte Makromolekulare Chemie: Appl. Macromol. Chem. Phys.*, vol. 232, no. 1, pp. 65–83, 1995.
[44] J. L. Hodgson and M. L. Coote, "Clarifying the mechanism of the denisov cycle: How do hindered amine light stabilizers protect polymer coatings from photo-oxidative degradation ?," *Macromolecules*, vol. 43, no. 10, pp. 4573–4583, 2010.
[45] M. R. Paine, G. Gryn'ova, M. L. Coote, P. J. Barker, and S. J. Blanksby, "Desorption electrospray ionisation mass spectrometry of stabilised polyesters reveals activation of hindered amine light stabilisers," *Polym. Degradation Stability*, vol. 99, pp. 223–232, 2014.
[46] A. Wypych and G. Wypych, *Databook of UV Stabilizers*. Scarborough, ON, Canada: ChemTec Publishing, 2020.
[47] J. Almond, P. Sugumaar, M. N. Wenzel, G. Hill, and C. Wallis, "Determination of the carbonyl index of polyethylene and polypropylene using specified area under band methodology with ATR-FTIR spectroscopy," *e-Polymers*, vol. 20, no. 1, pp. 369–381, 2020.
[48] G. Socrates, *Infrared and Raman Characteristic Group Frequencies: Tables and Charts*. Hoboken, NJ, USA: John Wiley & Sons, Inc., 2004.
[49] N. S. Allen, M. Edge, M. Rodriguez, C. M. Liauw, and E. Fontan, "Aspects of the thermal oxidation, yellowing and stabilisation of ethylene vinyl acetate copolymer," *Polym. Degradation Stability*, vol. 71, no. 1, pp. 1–14, 2000.
[50] G. Oreski, G. M. Wallner, and R. Lang, "Ageing characterization of commercial ethylene copolymer greenhouse films by analytical and mechanical methods," *Biosyst. Eng.*, vol. 103, no. 4, pp. 489–496, 2009.
[51] B. Ottersböck, G. Oreski, and G. Pinter, "Comparison of different microclimate effects on the aging behavior of encapsulation materials used in photovoltaic modules," *Polym. Degradation Stability*, vol. 138, pp. 182–191, 2017.
[52] C. Barretta, G. Oreski, S. Feldbacher, K. Resch-Fauster, and R. Pantani, "Comparison of degradation behavior of newly developed encapsulation materials for photovoltaic applications under different artificial ageing tests," *Polymers*, vol. 13, no. 2, 2021, Art. no. 271.
[53] Y. Shindo, B. Read, and R. Stein, "The study of the orientation of polyvinyl chloride films by means of birefringence and infrared, visible, and ultraviolet dichroism," *Die Makromolekulare Chemie: Macromol. Chem. Phys.*, vol. 118, no. 1, pp. 272–312, 1968.
[54] A. P. Patel, A. Sinha, and G. Tamizhmani, "Field-aged glass/backsheet and glass/glass PV modules: Encapsulant degradation comparison," *IEEE J. Photovolt.*, vol. 10, no. 2, pp. 607–615, Mar. 2020.
[55] J. H. Wohlgemuth, M. D. Kempe, and D. C. Miller, "Discoloration of PV encapsulants," in *Proc. IEEE 39th Photovolt. Specialists Conf.*, 2013, pp. 3260–3265.
[56] D. C. Miller et al., "Degradation in photovoltaic encapsulant transmittance: Results of the first PVQAT TG5 artificial weathering study," *Prog. Photovolt.: Res. Appl.*, vol. 27, no. 5, pp. 391–409, 2019.
[57] Y. Lyu et al., "Fluorescence imaging analysis of depth-dependent degradation in photovoltaic laminates: Insights to the failure," *Prog. Photovolt.: Res. Appl.*, vol. 28, no. 2, pp. 122–134, 2020.
[58] N. Pinochet, R. Couderc, and S. Therias, "Solar cell UV-induced degradation or module discolouration: Between the devil and the deep yellow sea," *Prog. Photovolt., Res. Appl.*, 2023.